FINITE ELEMENT MODELLING AND EXPERIMENTAL VERIFICATION OF TWO-WAY SANDWICH PANELS MADE OF NATURAL FIBER COMPOSITES

Dillon Betts[1]*, Pedram Sadeghian[2], and Amir Fam[3]

[1] PhD Candidate, Department of Civil and Resource Engineering, Dalhousie University, 5268 DaCosta Row, Halifax, NS B3H 4R2, Canada.

[2] Associate Professor and Canada Research Chair in Sustainable Infrastructure, Department of Civil and Resource Engineering, Dalhousie University, 5268 DaCosta Row, Halifax, NS, B3H 4R2, Canada.

[3] Donald and Sarah Munro Chair Professor in Engineering and Applied Science and Associate Dean (Research), Department of Civil Engineering, Queen's University, Kingston, ON, K7L 3N6, Canada.

** corresponding author, email: dillonbetts@dal.ca*

DOI: http://dx.doi.org/10.1061/JCCOF2.CCENG-3897

ABSTRACT: Finite element (FE) modelling of sandwich panels with bidirectional flax fibre-reinforced polymer (FFRP) faces and polyisocyanurate foam cores in two-way bending under concentrated loads was performed. Additionally, three large scale (1200 x 1200 mm) sandwich panels with FFRP faces of various thicknesses (one, two or three layers of flax fabric) and 75 mm thick foam cores were tested under a concentrated load. The modelling was completed using the commercially available software. The material nonlinearity of both the FFRPs and the foam cores was considered as well as the geometric nonlinearity due to localized deformation. Four failure modes were considered, FFRP compression crushing, FFRP tensile rupture, core shear and compression face wrinkling. Using the verified model, a parametric study investigated the effect of foam core density, face thickness, core thickness and the size of the loading area. It was found that panels with low density cores were more susceptible to face wrinkling failure while panels with high density cores are susceptible to both tensile rupture and core punching shear

failure. It was also shown that an increase in the diameter of the loading area lessened the effect of localized deformation for panels with high density (96 kg/m^3) cores.

KEYWORDS: Sandwich Structures, Flax Fibres, Bio-resins, Experimental Testing, Finite Element Modelling

INTRODUCTION

Sandwich panels are efficient structures made of two relatively strong and stiff faces separated by a lightweight core. The separation of the two faces provided by the core increases the moment of inertia which gives these panels a high stiffness and flexural rigidity. The faces resist the majority of the bending force, while the core resists shear force. As lightweight foams with high insulative properties can be used as the core material, these structures are ideal for applications where light weight and high insulation are required, such as building cladding materials. Sandwich panels have also been successfully used for roofing panels.

As the exterior face of buildings, cladding systems are subjected to environmental loads. During storm events, building cladding must withstand quasi-static wind pressures, dynamic wind gusts and, additionally, there is the potential of impact loads from wind-borne debris. Therefore, it is important to understand the behaviour of sandwich panels under uniform loading as well as concentrated forces, due to the potential for large mass, low velocity impacts. This paper focuses on the behaviour of sandwich panels under quasi-static concentrated forces.

As the core material is typically significantly weaker than the face materials, the capacity of these structures is often limited by the core strength. Traditional sandwich panel faces include aluminium, glass fibre-reinforced polymers (GFRPs) and carbon fibre-reinforced polymers (CFRPs). While glass and carbon fibres are considered sustainable options for infrastructure applications, they are manufactured materials and therefore require energy to be produced. Natural flax fibres have lower strength and stiffness than the more traditional glass and carbon fibres but offer a lower embodied energy (Cicala et al. 2010; Mak et al. 2015) and are a renewable resource. For sandwich panels, the full strength of GFRP and CFRP faces is often underutilized due to the shear strength limitations of typical core materials, such as foam. Therefore, as the strength of the face material does not typically govern sandwich panel failure, flax fibre-reinforced polymers (FFRPs) are a feasible sustainable alternative for the face material. The material properties of FFRPs and other natural fibre-reinforced polymers have been investigated and the results show that they exhibit a nonlinear stress-strain response (Betts et al. 2018; Christian and Billington 2011; Sadeghian et al. 2018). Therefore, to accurately predict the behaviour of sandwich panels with natural FRP faces, it is important to consider their nonlinear mechanical behaviour. Additionally, it is important to consider the geometric nonlinearity of the sandwich panels under localized loads.

Sandwich panels with traditional face materials have been studied extensively using finite element (FE) modelling under quasi-static loads (Dawood et al. 2010; Satasivam et al. 2018; Sharaf and Fam 2012) and impact loads (Besant et al. 2001; Feng and Aymerich 2013; Meo et al. 2005; Zhang et al. 2016; Zhou et al. 2012). Dawood et al (2010) tested and numerically modelled two-way 1220 mm x 1220 mm x 25 or 50 mm thick sandwich structures with GFRP faces and foam cores. They used an FE model paired with a rational analysis to develop a simplified analysis procedure with which they performed a parametric study. Sharaf and Fam (2012) developed a numerical FE model to predict the one-way bending behaviour of sandwich panels with GFRP faces and foam cores with and without ribs. Their model accounted for material and geometric nonlinearity and was validated against experimental data. The model was then used to determine the most efficient GFRP rib configuration of the panels. Sandwich panels have also been investigated using fiber element modelling (Fam et al. 2016). In this study Fam et al (2016) examined the behaviour of one-way sandwich beams with glass FRP faces and soft cores and looked at the effect of shear deformation of the core on the behaviour of the sandwich beams. They showed that both face thickness and core density affected the failure modes observed in the beams and that as the core density increased from low density (32 kg/m^3) to high density (192 kg/m^3), the contribution of shear deflection decreased significantly.

Recently, FFRP-foam sandwich panels have been investigated under flexural loads (Betts et al. 2018; Mak et al. 2015; Mak and Fam 2019; Sadeghian et al. 2018), axial loads (Codyre et al. 2016) and impact loads (Betts et al. 2020, 2021). Some studies have been completed on experimental and FE modelling of FFRP-cork sandwich panels under impact loads (Boria et al. 2018). However, in the study by (Boria et al. 2018), the nonlinear behaviour of the FFRP faces was not considered. There are currently no studies providing an in-depth look at the behaviour of FFRP-foam sandwich structures under flexural loads using FE modelling. Additionally, there is a major gap in the literature concerning the two-way behaviour of sandwich structures with FFRP faces. In this study, FE models considering the material and geometric nonlinearity of the two-way behaviour of FFRP-foam sandwich panels are developed and verified using experimental data. Then, the modelling program is expanded to perform a parametric study to determine the effect of face thickness, foam core density and the load area size on the flexural and shear behaviour of large-scale sandwich panels with FFRP faces and foam cores.

FE MODEL DEVELOPMENT

The finite element modelling presented in this study was performed using the implicit solver of the program (Livermore Software Technology Corporation (LSTC) n.d.). The models were developed using 3D solid elements with element formulation -2, as suggested in the implicit guideline from Dynamore (2018). This is an accurate element formulation for fully integrated S/R solid elements with poor aspect ratios. To lessen the computational effort required, only a quarter of the panels were modelled assuming a roller support on each side. A photo of the 3FL sandwich panel model is presented in Figure 1. In this section, material models, boundary conditions and mesh sizes will be presented and discussed.

Material Properties

Materials Testing

The flax fibre-reinforced polymer (FFRP) faces were fabricated using a two-by-two twill bidirectional flax fabric and a bio-based epoxy resin. The flax fabric had a reported areal mass of 400 g/m^2 (measured at 410 g/m^2). The bio-based epoxy resin used had an approximate bio-content of 25%. The epoxy properties were determined in a previous study by Betts et al (2018) using ASTM D638 (2014). Their tests showed that the epoxy had a mean (± coefficient of variation) tensile strength, initial elastic modulus and ultimate strain of 57.9 MPa ± 0.6 %, 3.20 GPa ± 4.0% and 0.0287 mm/mm ± 6.3%, respectively.

The tensile properties of the bidirectional FFRPs were determined in both the warp and weft directions using ASTM D3039 (2017) and the shear properties were found using ASTM D3518 (2018a). For each test type, five identical 250 mm x 25 mm coupons were tested. The tension coupons were comprised of two layers of flax fabric whereas the shear coupons comprised of four layers of flax fabric. The coupons were all fabricated using a wet lay-up procedure. The tensile strength, initial elastic modulus and ultimate strain (± coefficient of variation) were found to be 70.0 MPa ± 4.9%, 6.35 GPa ± 11.2% and 0.0202 mm/mm ± 10.9%, respectively, in the warp direction and 51.3 MPa ± 2.7%, 5.64 GPa ± 16.0% and 0.0204 mm/mm ± 11.8%, respectively, in the weft direction. The difference between stress-strain behaviour in the warp and weft directions has also been observed in hemp FRPs and has been attributed to higher yarn crimp in the weft direction (Christian and Billington 2011). The shear strength, shear modulus and ultimate shear strain were found to be 23.1 MPa ± 1.7%, 1.26 GPa ± 1.6%, and 0.0562 mm/mm

± 9.4%, respectively. The stress-strain responses in tension and shear were averaged and are presented in Figure 2.

The shear properties of the foams were determined experimentally using ASTM C273 (2018b). Five identical 240 mm long, 50 mm wide and 20 mm thick specimens were tested. The shear strength, shear modulus and ultimate shear strain of the 96 kg/m^3 polyisocyanurate foam were found to be 0.476 MPa ± 21.4%, 12.5 MPa ± 6.4% and 0.59 mm/mm ± 3.1%, respectively. The shear stress-strain behaviour and photos of the test set-up and a typical failure are presented in Figure 3.

Material Models

The two-ply bidirectional FFRP coupons tested had an average thickness of 2.34 mm. Therefore, the faces were modelled based on this thickness. The one flax layer (1FL) specimen faces were modelled as 1.17 mm thick; the (two flax layer) 2FL specimen faces were modelled as 2.34 mm thick and the (three flax layer) 3FL specimen faces were modelled as 3.51 mm thick.

In order to capture the nonlinear behaviour shown in Figure 2. the FFRP faces were modelled using MAT_040, NONLINEAR_ORTHOTROPIC. This material model takes the material stress-strain curves as inputs and therefore is able to accurately predict the behaviour of the FFRPs in both the warp and weft direction. However, this material model is not able to include material damage or failure. To verify this material model, a tension coupon was modelled in both the warp and weft direction and compared to the test data. This verification is presented in Figure 4.

It is also known that the FFRPs behave differently under tensile and compressive loads (Betts et al. 2018). However, the material model used is unable to account for this difference. Therefore, knowing that for quasi-static loads, the top face is generally under compression and the bottom face is generally under tension, the top face was modelled using the warp compressive stress-strain data from Betts et al. (2018) and the bottom face was modelled using the tensile stress-strain data shown in Figure 2. The FFRPs in the warp direction were found have an initial compressive modulus of 6.73 GPa and a compressive strength and corresponding strain of 86.4 MPa and 0.0327 mm/mm (Betts et al. 2018).

The core was modelled using material model MAT_057, LOW_DENSITY_FOAM. This model takes the compressive stress-strain curve of the foam as an input. The stress-strain curve for the 96 kg/m^3 PIR foam presented by Codyre et al (2018) was used for the modelling.

The supports were modelled as steel using the MAT_001, ELASTIC. The loading disc was also made of steel, but was modelled as MAT_020, RIGID. This allowed for the use of the prescribed motion boundary condition that can be used with rigid parts. The rubber beneath the loading disc was modelled as MAT_007, BLATZ-KO_RUBBER with a shear modulus, G, of 15 MPa. However, the actual shear modulus of the rubber pad used in the tests is not known.

Contacts and Boundary Conditions

The faces of the sandwich panel were connected to the core in the model using a tied mortar contacts. Tiebreak contacts were not used because there was no separation between face and core material observed during the experimental tests. As noted by the implicit guidelines (Dynamore 2018), solid to solid mortar contacts can lead to noticeably large penetrations. In the guideline, it is suggested that increasing the contact penalty stiffness can alleviate this problem, however it may lead to convergence problems. To increase the penalty stiffness, two parameters can be changed: the scale factor on default slave penalty stiffness (SFS) and the IGAP parameter. The IGAP parameter controls how quickly the penalty force increases due to penetration distance. In the model presented in this study, the penalty stiffness for the contacts was increased from the default by setting SFS = 5 and IGAP = 5.

To take advantage of symmetry, it was assumed that the supports were roller-type supports in both directions. Figure 5 shows the modelling of the panel supports. They were modelled with solid elements which were allowed to rotate about the bottom centerline as shown in the figure. These supports were connected to the panel using automatic surface to surface mortar contacts which allowed the panel to slide simulating a roller behaviour. This sliding was allowed by setting the coefficient of friction of the contact to a low value of 0.0001. This value was set as an arbitrary low value not equal to zero, such as not to cause any computational problems. The panels were also allowed to separate from the supports. This is important because the corners of two-way panels often lift off the supports when subjected to flexural loads. It should be noted that in the tests, two of the roller supports were welded to the support frame to simulate a pin-type support. However, it was assumed that this simplification would not significantly affect the model results and allowed the computational effort to be reduced by a factor of four. To use the quarter model, the cut edges required special boundary conditions due to symmetry. In the cut along the *yz*-plane, the nodes were restricted from moving in the *x*-direction and likewise, in the *xz*-plane, the nodes were restricted from moving in the *y*-direction.

The load was applied to the panel through a steel loading disc which was placed on a rubber pad. Between both the loading disc and the rubber pad and between the rubber pad and the panel, automatic surface to surface mortar contacts were used. For these contacts the static coefficient of friction was assumed to be 0.8. Using the 3FL-C96 model, static friction coefficient values of 0.01, 0.2, 0.4 and 0.6 were also investigated. It was determined that its overall effect on the model was insignificant, but that the value of 0.8 provided the most accurate load-strain slopes and therefore it was chosen.

Failure Modes

Failure was considered in the post-processing of the model using a script written in Python using the scientific package, Anaconda. Material failure was considered in both the FFRP faces and the PIR foam core and the stability type failure, face wrinkling was considered on the top face.

To check for material failure in the faces, the maximum stress criterion was used. The normal stresses in elements at the center of the top and bottom faces were exported from the model. Then, a python script checked the stress in the warp (y) and weft (x) directions at each model step. The stresses were checked against both the compressive and tensile strength of FFRP. If, at any point, the stress in any direction exceeded the ultimate material strength, the model was terminated and the failure mode noted.

The foam core was checked for shear failure using the Tresca failure criterion (Gere 2008). As shown in Figure 6b, it was observed that, for a 3FL-C96 sandwich panel, shear failure began at the edge of the loading disc. This is an expected result as stress concentrations typically develop at the edge of the load applications. From this initialization of foam shear failure, the failure area propagated downward as shown in Figure 6c. Total failure due to foam shear was then assumed when the maximum shear stress (Tresca) exceeded the ultimate shear stress of the foam in over half the thickness of the foam, as shown in Figure 6d. To implement this failure mechanism into the post-processing, the Tresca stress in the element just below the midplane of the core was exported from the model. In the case of the 3FL-C96 panel, this is the element shown in Figure 6d. The core was considered to have failed when the Tresca stress in this element exceeded the ultimate shear strength of foam material.

Compression face wrinkling failure was considering using the critical stress equation presented by Allen (1969) and given by Eq. 1:

$$\sigma_{cr} = B_1 E_f^{1/3} E_c^{2/3} \tag{1}$$

where σ_{cr} is the critical compressive stress in the face causing wrinkling, B_1 is a parameter given by Eq. 2, E_f is the elastic modulus of the face and E_c is the elastic modulus of the core. Because

FFRPs exhibit a nonlinear behaviour, the elastic modulus was taken conservatively as the ultimate secant modulus, that is: $E_f = \sigma_{fu} / \epsilon_{fu}$, where σ_{fu} is the ultimate strength of the FFRP and ϵ_{fu} is the ultimate strain of the FFRP.

$$B_1 = 3[12(3-\nu_c)^2(1+\nu_c)^2]^{1/3} \quad (2)$$

where ν_c is the Poisson's ratio of the core material. For the PIR foams used in this study, the Poisson's ratio is not known and therefore a typical value of 0.3 was chosen. Allen (1969) showed that B_1 is not significantly affected by the Poisson's ratio and therefore this assumption does not have a significant effect on the prediction of the critical wrinkling stress. The stress history for the element exhibiting the highest compressive stress in each direction was exported from the model and checked at each model step. If the compressive stress was found to be greater than the critical stress, the model was considered to have failed.

As shown in Figure 3, the average (± standard deviation) ultimate foam shear stress, $\tau_{cu,a}$, of the 96 kg/m^3 foam was to be 0.476 ± 0.102 MPa. Because the tests showed a high variance in strength, a region of potential total shear failure was determined. The lower bound, $\tau_{cu,l}$, of the potential shear failure was set as the average shear strength minus one standard deviation and the upper bound, $\tau_{cu,u}$, was set as the average plus one standard deviation. Each point was noted in the post processing and if the Tresca stress exceeded the upper bound, it was assumed that the panel failed due to core shear.

Mesh Convergence

To determine the most appropriate mesh, a mesh size convergence study was performed on both the 3FL and the 1FL specimen. The study was performed on these two specimens, to ensure that the effect of the mesh size was observed for both failure of the face material (1FL) and for failure of the core material (3FL). Four meshes were considered as presented in Figure 7: a coarse mesh (Coarse), a refined coarse mesh (Coarse-R), a refined moderate mesh (Moderate-R) and a refined fine mesh (Fine-R).

The mesh size analysis for the 1FL and 3FL-C96 sandwich panels are shown in Figure 8 and Figure 9, respectively. As shown in Figure 8 the ultimate load capacity decreased with a decrease in mesh size (i.e. changing from Coarse to Fine-R). The smallest percentage decrease in ultimate load capacity was 3.1% between Moderate-R and Fine-R whereas the decreases between Coarse and Coarse-R, and Coarse-R and Moderate-R were 5.4% and 5.8%, respectively. Figure 8 also shows that the mesh size did not have a significant effect on the initial stiffness of the panels.

Figure 9 shows the effect of the mesh size on the ultimate capacity, initial stiffness and computational runtime for the 3FL-C96 panels. As the shear failure is predicted as a region, the mesh size effect was presented for the average shear failure capacity as well as the lower and upper bounds. As shown in the figure, there was no significant effect on the average core shear failure load, the maximum difference was 3.1% between the Coarse-R mesh and the Moderate-R mesh. Additionally, Figure 9a shows that the initial stiffness increased slightly with a decrease in mesh size. Figure 9b shows the effect of the mesh size on the computational runtime of the 3FL-C96 specimen. As the mesh size decreases, the runtime increases significantly, especially between the Moderate-R and Fine-R meshes. Therefore, to ensure accurate results for specimens failing due to face rupture (as panel 1FL-C96) while maintaining a reasonable computational runtime, the Moderate-R mesh was selected for the model verification and parametric study.

EXPERIMENTAL PROGRAM

To verify the model, three large scale two-way sandwich panels were fabricated and tested under a concentrated load at the center. The sandwich panels were comprised of flax fibre-reinforced polymer faces and polyisocyanurate foam cores with a density of 96 kg/m^3. Each sandwich panel was 1220 mm by 1220 mm and approximately between 78 and 85 mm thick. The main test parameter was the effect of face thickness, namely one, two or three layers of flax fabric per face.

Specimen Fabrication

The specimen fabrication procedure for each panel is presented in Figure 10. The 75 mm thick foam was supplied in 2400 mm by 1220 mm panels. The foam was cut to 1220 mm by 1220 mm using a circular saw. The foam surface was cleared of any dust and debris using a bristle brush. A layer of epoxy was evenly applied to the surface of the foam (Figure 10b). Then, a layer of the bidirectional flax fabric was placed on the specimen (Figure 10c) and the warp direction was recorded on the side of the foam. A plastic scraper was then used to gently press the fabric into the epoxy layer below (Figure 10d). Then, a layer of epoxy was evenly applied to the flax fabric (Figure 10e). These last three steps were repeated as necessary to achieve different face thicknesses, namely, one two or three layers. Note that all layers were placed with the warp direction of the fabric along the same axis. This was done to allow for a direct comparison between the sandwich panels with one face layer and multiple face layers. Sheets of parchment paper were applied in the warp direction of the fabric and an aluminum roller or plastic scraper was used to remove any air and excess epoxy (Figure 10f). A weighted board was then placed on the specimen (Figure 10g) and the face was allowed to cure for 24 hours under the weighted board. After 24 hours, the opposite face was completed following the same procedure. After seven days of curing at room temperature, the edges of the faces were cut flush using a jig saw (Figure 10h). After fabrication, all specimens were stored in a dry environment until testing.

Test Set-up and Instrumentation

Figure 11 shows the test set-up. The load was applied to the center of 1220 mm by 1220 mm sandwich panel specimen using a hydraulic actuator through a 150 mm diameter steel disc. To protect the wires of the strain gauges, a piece of rubber was placed under the applied load. The sandwich panel was supported by steel roller supports on a steel frame which sat on a concrete strong floor. In each direction, one of the steel rollers was welded to the frame to simulate a pin connection.

The data instrumentation layout is presented in Figure 12. The load was measured using a 250 kN load cell and the center deflection was measured using a string potentiometer connected to the sandwich panel on the bottom face. Additionally, four linear potentiometers (LPs) measured the deflection at the quarter points of the panel, that is, halfway between the panel center and the corners of the supports. Strain gauges with a 6 mm gauge length and a resistance of 350-ohms measured the strain in the warp, weft and 45° directions at the center on both the top and bottom faces. All data was measured at a sample rate of 10 samples per second.

Experimental Results

The failure modes of the quasi-static tests are shown in Figure 13. As the face thickness increased, the failure mode transitioned from a tension face-controlled failure (1FL-S) to a core shear failure, which lead to local failure of the compression face (3FL-S). Specimen 2FL-S failed due to tension at the bottom face. However, the top face showed signs of the start of local failure, as evidenced by the light colouring around the load area of the top face shown in Figure 13b, and therefore it is assumed that this specimen was close to the core shear failure as well.

The results of the quasi-static tests are presented in Figure 14 and Table 1. As shown in Figure 14a, the ultimate strength and stiffness of the panels increased with face thickness. Note that the panel stiffnesses were considered as the slope of the first initial portion of the load-deflection diagrams. The load-deflection diagrams also show that there was a larger increase in both strength and stiffness between specimens 1FL-S and 2FL-S than between 2FL-S and 3FL-S. The ultimate strength and initial stiffness increased by 78% and 51%, respectively, between specimens 1FL-S and 2FL-S. However, the ultimate strength and initial stiffness only increased by 12% and 4%, respectively, between specimens 2FL-S and 3FL-S. This is likely caused by the more prominent effect of shear and local deformations of the 2FL-S and 3FL-S panels, which is shown in the load-strain diagrams shown in Figure 14b. The load-compression strain curves show the top faces of the 2FL-S and 3FL-S panels started the tests by going into a state of compressive strain, as expected. At a load of approximately 29 kN, the compression strain in the top faces began to decrease due to the presence of localized tensile strain under the loading disc. This is indicative of local indentation under the load application. Additionally, as the FFRP face thickness increased, shear became the more prominent global deformation mode. This transition from bending (face-controlled) deformation to shear (core-controlled) deformation means that the face thickness has a less significant effect on the overall stiffness of the plate.

Model Verification

Table 1 shows the comparisons of the ultimate loads and ultimate deflections, initial stiffnesses and failure modes between the models and the tests. As shown in Table 1, the average model-test ratio for the prediction of ultimate load and deflection are 0.96 and 0.97, respectively. Additionally, the failure mode was accurately predicted for the 1FL-C96 and 3FL-C96 specimens. Visual comparisons of the model and test failure modes for the 1FL-C96 and 3FL-C96 specimens are presented in Figure 15 and Figure 16, respectively. Note that in Figure 15, the cracks on the 1FL test specimen extend from edge to edge, predominantly in the weft direction. However, the model only captures the onset of the cracking due to the high stress in the center of the bottom face.

Upon examination of the model results, 2FL-C96 specimen was close to a balanced failure point between core shear failure and bottom face tensile rupture. At failure, the stress in the weft direction of the bottom face was 50.0 MPa, which is 97.5% of the ultimate strength.

Figure 17 shows a comparison of the load-deflection and load-strain behaviour of the models and experiments. Though Table 1 indicates that the initial stiffness was slightly under-predicted by the models, Figure 17 shows that the overall slopes of the load-deflection diagrams were predicted well. As shown in the figure, the slope of the 1FL-C96 experimental specimen seems to gain stiffness at the beginning of the stress-strain curve and this behaviour is not captured by the model. However, a stiffness increase is not expected in these panels, and it is likely that this was caused by some settlement in the test apparatus. The figure also shows that the model was able to accurately predict the strain behaviour at the center of the top face. However, note that the transition to a state of tensile strain in the top face is more sudden in the FE tests than in the experimental data. This is likely due to the use of the LOW_DENSITY_FOAM material model which is based on the compressive stress-strain curve of the foam. In future studies, it is recommended that other material models be tested to determine the most accurate model for PIR foams. Based on the information presented in this section, this two-way model can be considered successfully verified when using the upper bound of the shear failure region. Therefore, for the remainder of this paper, the upper bound of the shear failure region will be considered as the failure criteria.

PARAMETRIC STUDY

A parametric study was performed using the verified model to observe the effect of the core density, face thickness and the load area diameter on the behaviour of the panels. In this section, the results of the parametric study will be presented and discussed. Additionally, the material models for the different core densities will be verified. Note that, while the parametric study presented in this paper provides some understanding of the behaviour of two-way sandwich panels with FFRP faces, a more in-depth parametric study should be performed in future research with a focus on developing design equations for these panels.

Verification of Additional Foam Material Models

For the parametric study, the behaviour of sandwich panels with two additional PIR foam core densities were investigated: 32 kg/m^3 and 64 kg/m^3. These additional foams were modelled using their respective compressive stress-strain curves presented by Codyre et al (2018). In their study, they showed that the compressive moduli of the C32, C64 and C96 foams were 4.9 MPa, 12.6 MPa and 35.1 MPa, respectively (CoDyre et al. 2018). However, they did not perform any shear tests and therefore the manufacturer data (Elliott Company 2016a; b) was used to predict core shear failure. The manufacturer data provides shear strength parallel to the rise of the foam and perpendicular to the rise of the foam. These two values were used to predict a shear failure region and it was assumed that the larger of the two caused ultimate shear failure.

To accurately model panels with these additional core densities, the material models for the foams first had be verified. This was done by modifying the two-way FE model to examine the behaviour of the sandwich beams tested by Betts et al (2018) and fabricated using the three different core densities. This beam model is presented in Figure 18. Note that to save on computational time, the principle of symmetry was used to model half of the beam length. Additionally, because the beams are under a state of plane stress, only a third of the beam width was modelled.

The comparisons of the load-deflection behaviour of the FE beam models and the tests by Betts et al (Betts et al. 2018) is presented in Figure 19. The figure shows that the behaviour of the beams was predicted accurately by the FE models. Therefore, the foam material models can be used to perform the parametric study of the two-way panels.

Effect of Core Density

The effect of core density on the ultimate load, ultimate deflection and initial stiffness of the two-way sandwich panels is presented in presented in Table 2 and Figure 20. Figure 20a shows that the ultimate load capacity increases with core density for all face thicknesses. Note that the increase is not linear as it is affected by the failure mode. As shown in Table 2, the failure of the C32 and C64 panels was due to compression face wrinkling and for the C96 specimens the failures were due to tensile rupture or core shear. The core density did not have a significant effect on the ultimate deflection for the 1FL and 2FL panels. However, the ultimate deflections of the 3FL panels decreased with an increase in core density.

Figure 21 shows the effect of panel core density on the load-deflection and load-strain behaviour of two-way the sandwich panels. The load-deflection diagrams for the panels with lower density cores (32 kg/m^3) showed an increasing slope until failure. As the compressive yield stress and modulus of the 32 kg/m^3 foam is significantly less than the 96 kg/m^3 foam, it is assumed that this stiffness gain is attributed to densification of the foam under the load area. Specifically, this densification would occur under the edge of the load area.

As shown in Figure 21, the initial load-face strain behaviour is similar for all core densities. For all panels other than 1FL-C96, the strains in the top face transition into a state of tensile strain. This phenomenon was discussed earlier, and it was assumed that this was caused by the onset of local deformation. The results of the models confirm this hypothesis and show that this behaviour is specifically due to the onset of core indentation under the edge of the load area. Because the yield stress and compressive moduli of the cores decrease with core density, this indentation starts at lower load levels for the lower density foams. Therefore, the transition from compression to tensile strain at the center of the top face occurs at an earlier stage for the panels with the lower density cores, as shown in Figure 21.

Effect of Face Thickness

The effect of face thickness on the ultimate load capacity, ultimate deflection and initial stiffness of the two-way sandwich panels is presented in Table 2 and Figure 20b. The ultimate load capacity increased with an increase in the number of FFRP layers per face. For the C96 panels, the increase between one and two layers of FFRP is more significant than the increase between two and three layers. This is due to the failure modes of the panels. As the 1FL-C96 panel failed due to tensile rupture and it has been shown that 2FL-C96 panel was close to tensile rupture before ultimately failing due to core shear, the ultimate capacity is largely dependent on the face thickness. However, as the 2FL-C96 and 3FL-C96 panels both failed due to core shear, the increase in FFRP layers per face has a less significant effect on the ultimate panel capacity. Similarly, the ultimate deflections of the C96 panels were not significantly affected by the face thickness. However, both the ultimate load and displacement of the C32 and C64 panels increased with an increase in face thickness. This is expected as these panels failed due to compression face wrinkling which is affected by both the face and core material properties. The initial stiffness of all panels increased with the number of FFRP layers per face.

By comparing the plots in Figure 21, it can be seen that the slope of the load-strain diagrams increased with an increase in face thickness. Additionally, the amount of compressive strain experienced by the top faces decreased with an increase in face thickness.

Effect of Load Area Diameter

To develop an understanding of the effect of the load area diameter, additional models were developed for the C96 panels. As shown in Figure 22, three load size diameters were considered: 150 mm (original), 300 mm and 600mm. The only change implemented in the models was the size of the loading disc, that is that the contact formulations, material models and boundary conditions were not altered. Note that, as they are quarter models, the load sizes shown in Figure 22 are half of the load area diameters.

The effect of load area diameter on the ultimate load capacity, ultimate deflection and initial stiffness of the two-way sandwich panels is presented in Table 2 and Figure 20c. Additionally, the effect on the load-displacement and load-face strain behaviour is presented in Figure 23. As expected, the ultimate load capacity and initial stiffness, increased with an increase in load area. The ultimate deflection of the 1FL-C96 specimens increased with an increase in the load area, however the 2FL-C96 and 3FL-C96 panels were relatively unaffected. This is due to the different failure modes of the panels as shown in Figure 13. The 1FL-C96 panels all failed due to tensile rupture of the bottom face whereas the 2FL-C96 and 3FL-C96 panels all failed due to core shear.

The slopes of the load-face strain plots were increased with an increase in the load area diameter. Additionally, Figure 23 shows that the top faces of the models with larger load areas (300 mm and 600 mm) did not go into a state of tensile strain. This is an expected result as the stress concentration developed at the edge of the load area is distributed over a larger perimeter.

Effect of Core Thickness

The effect of the core thickness was examined for sandwich panels with core densities of 96 kg/m^3. As shown in Figure 24, three core thicknesses were considered: 25.4 mm, 50.8 mm and 76.2 mm (as tested).

The effect of the core density on the load-displacement and load-strain behaviour of the sandwich panels is presented in Figure 25. The ultimate load capacity and stiffness increased with an increase in core thickness for all panels. For the 1FL panels, the ultimate center displacement also increased with a decrease in core thickness. However, for the 2FL and 3FL panels, the effect of core thickness on the ultimate displacement was not clear. As these panels failed due to core shear, it is likely that the ultimate displacement was heavily influenced by the localized deformation at the ultimate point. As shown in Figure 25, the slope of the load-strain increased with an increase in core thickness. This is expected as an increase in core thickness is an increase in moment of inertia, thereby increasing the flexural rigidity of the structure.

CONCLUSIONS

In this study, the behaviour of large-scale sandwich panels with flax fibre-reinforced polymer (FFRP) faces and foam cores under a concentrated load was examined numerically. From the experimental tests the following behaviours were noted:

- The ultimate strength and stiffness of the panels increased with face thickness. However, a larger difference in both strength and stiffness was observed between panels with one and two layers of FFRP per face than between specimens with two and three layers. This difference was attributed to a change from a face-controlled behaviour to a core-controlled behaviour.
- Localized deformations of the top face and core were observed under the loading area. This deformation affected the specimens with the thicker faces more than the panel with one layer of FFRP per face.

Finite element models were created using implicit solver of the commercially available program (Livermore Software Technology Corporation (LSTC) n.d.). Both the material nonlinearity of the FFRP faces and foam cores and the geometric nonlinearity were accounted for in the models. Material failure was considered in the faces using the maximum stress criterion and, in the core, using the Tresca failure criterion. Additionally, the stability type failure of compression face wrinkling, was considered in the top faces. The models were successfully verified and validated using test data.

A parametric study investigated the effect of the foam core density, the FFRP face thickness, the core thickness, and the size of the load area. Based on the parametric study the following conclusions were drawn:

- The models were able to accurately capture the strain state in the center of the top faces observed in the tests. The top faces started in a state of compression, but after the onset of indentation under the load edge, transitioned to a state of tensile strain.
- Panels examined experienced failure due to core shear, tensile rupture or compression face wrinkling. The failure modes were affected by both core density and face thickness, but not the load area diameter.
- Ultimate load capacity and initial stiffness both increased with and increase of core density, face thickness and load area diameter. Ultimate deflection was significantly affected by the failure modes and less so by the individual parameters.
- Increasing the size of the load area mitigated the effect of localized deformation under the load edge.

DATA AVAILABILITY

All data, models, or code that support the findings of this study are available from the corresponding author upon reasonable request.

ACKNOWLEDGEMENTS

The authors would also like to acknowledge and thank NSERC, Queen's University, and Dalhousie University for their financial support.

REFERENCES

Allen, H. G. 1969. *Analysis and Structural Design of Sandwich Panels*. Oxford, UK: Pergamon Press.

ASTM. 2014. "ASTM D638, Standard test method for tensile properties of plastics." *Annual Book of ASTM Standards*. West Conshohocken, Pennsylvania, US: ASTM International.

ASTM. 2017. "ASTM D3039/D3039M - Standard Test Method for Tensile Properties of Polymer Matrix Composite Materials." *Annual Book of ASTM Standards*. West Conshohocken, Pennsylvania, US: ASTM.

ASTM. 2018a. "ASTM D3518/D3518M, Standard Test Method for In-Plane Shear Response of Polymer Matrix Composite Materials by Tensile Test of a ± 45° Laminate." *Annual Book of ASTM Standards*. West Conshohocken, Pennsylvania, US: ASTM International.

ASTM. 2018b. "ASTM C273/C273M, Standard Test Method for Shear Properties of Sandwich Core Materials." *Annual Book of ASTM Standards*. West Conshohocken, Pennsylvania, US: ASTM International.

Besant, T., G. A. O. Davies, and D. Hitchings. 2001. "Finite element modelling of low velocity impact of composite sandwich panels." *Composites - Part A: Applied Science and Manufacturing*, 32 (9): 1189–1196. https://doi.org/10.1016/S1359-835X(01)00084-7.

Betts, D., P. Sadeghian, and A. Fam. 2018. "Experimental Behavior and Design-Oriented Analysis of Sandwich Beams with Bio-Based Composite Facings and Foam Cores." *Journal of Composites for Construction*, 22 (4): 1–12.

Betts, D., P. Sadeghian, and A. Fam. 2020. "Experiments and nonlinear analysis of the impact behaviour of sandwich panels constructed with flax fibre-reinforced polymer faces and foam cores." *Journal of Sandwich Structures and Materials*. https://doi.org/10.1177/1099636220925073.

Betts, D., P. Sadeghian, and A. Fam. 2021. “Post-Impact Residual Strength and Resilience of Sandwich Panels with Natural Fiber Composite Faces.” *Journal of Building Engineering*, 38: 102184.

Boria, S., E. Raponi, F. Sarasini, J. Tirillò, and L. Lampani. 2018. “Green sandwich structures under impact: experimental vs numerical analysis.” *Procedia Structural Integrity*, 12: 317–329. Elsevier B.V. https://doi.org/10.1016/j.prostr.2018.11.084.

Christian, S. J., and S. L. Billington. 2011. “Mechanical response of PHB- and cellulose acetate natural fiber-reinforced composites for construction applications.” *Composites Part B*, 42 (7): 1920–1928. Elsevier Ltd. https://doi.org/10.1016/j.compositesb.2011.05.039.

Cicala, G., G. Cristaldi, G. Recca, and A. Latteri. 2010. “Composites Based on Natural Fibre Fabrics.” *Woven Fabric Engineering*, P. D. Dubrovski, ed. IntechOpen.

Codyre, L., K. Mak, and A. Fam. 2016. “Flexural and axial behaviour of sandwich panels with bio-based flax fibre-reinforced polymer skins and various foam core densities.” *Journal of Sandwich Structures and Materials*, 1–22. https://doi.org/10.1177/1099636216667658.

CoDyre, L., K. Mak, and A. Fam. 2018. “Flexural and axial behaviour of sandwich panels with bio-based flax fibre-reinforced polymer skins and various foam core densities.” *Journal of Sandwich Structures and Materials*, 20 (5): 595–616. https://doi.org/10.1177/1099636216667658.

Dawood, M., E. Taylor, and S. Rizkalla. 2010. “Two-way bending behavior of 3-D GFRP sandwich panels with through-thickness fiber insertions.” *Composite Structures*, 92 (4): 950–963. Elsevier Ltd. https://doi.org/10.1016/j.compstruct.2009.09.040.

Dynamore. 2018. “Guideline for implicit analyses using LS-DYNA.” Dynamore.

Elliott Company. 2016a. “ELFOAM P400 Polyisocyanurate Foam.” Indianapolis, IN: Elliott Company.

Elliott Company. 2016b. “ELFOAM P200 Polyisocyanurate Foam.” Indianapolis, IN: Elliott Company.

Fam, A., T. Sharaf, and P. Sadeghian. 2016. “Fiber element model of sandwich panels with soft cores and composite skins in bending considering large shear deformations and localized skin wrinkling.” *Journal of Engineering Mechanics*, 142 (5): 1–14. https://doi.org/10.1061/(ASCE)EM.1943-7889.0001062.

Feng, D., and F. Aymerich. 2013. “Damage prediction in composite sandwich panels subjected to low-velocity impact.” *Composites Part A: Applied Science and Manufacturing*, 52: 12–22. Elsevier Ltd. https://doi.org/10.1016/j.compositesa.2013.04.010.

Gere, J. M. 2008. “Mechanics of Materials.” *Mechanics of Materials*, 913. https://doi.org/10.1016/j.mechmat.2009.01.011.

Livermore Software Technology Corporation (LSTC). n.d. “LS DYNA.”

Mak, K., and A. Fam. 2019. “Performance of flax-FRP sandwich panels exposed to different ambient temperatures.” *Construction and Building Materials*, 219: 121–130. Elsevier Ltd. https://doi.org/10.1016/j.conbuildmat.2019.05.118.

Mak, K., A. Fam, and C. Macdougall. 2015. “Flexural Behavior of Sandwich Panels with Bio-FRP Skins Made of Flax Fibers and Epoxidized Pine-Oil Resin.” *Journal of Composites for Construction*, 19 (2003): 1–13. https://doi.org/10.1061/(ASCE)CC.1943-5614.0000560.

Meo, M., R. Vignjevic, and G. Marengo. 2005. “The response of honeycomb sandwich panels under low-velocity impact loading.” *International Journal of Mechanical Sciences*, 47 (9): 1301–1325. https://doi.org/10.1016/j.ijmecsci.2005.05.006.

Sadeghian, P., D. Hristozov, and L. Wroblewski. 2018. “Experimental and analytical behavior of sandwich composite beams: Comparison of natural and synthetic materials.” *Journal of Sandwich Structures and Materials*, 20 (3): 287–307. https://doi.org/10.1177/1099636216649891.

Satasivam, S., Y. Bai, Y. Yang, L. Zhu, and X. L. Zhao. 2018. “Mechanical performance of two-way modular FRP sandwich slabs.” *Composite Structures*, 184 (March 2017): 904–916. Elsevier. https://doi.org/10.1016/j.compstruct.2017.10.026.

Sharaf, T., and a. Fam. 2012. “Numerical modelling of sandwich panels with soft core and different rib configurations.” *Journal of Reinforced Plastics and Composites*, 31 (11): 771–784. https://doi.org/10.1177/0731684412445494.

Zhang, D., D. Jiang, Q. Fei, and S. Wu. 2016. “Experimental and numerical investigation on indentation and energy absorption of a honeycomb sandwich panel under low-velocity impact.” *Finite Elements in Analysis and Design*, 117–118: 21–30. Elsevier. https://doi.org/10.1016/j.finel.2016.04.003.

Zhou, J., M. Z. Hassan, Z. Guan, and W. J. Cantwell. 2012. “The low velocity impact response of foam-based sandwich panels.” *Composites Science and Technology*, 72 (14): 1781–1790. Elsevier Ltd. https://doi.org/10.1016/j.compscitech.2012.07.006.

Table 1. Verification of FE models using test data

	Ultimate Load [1], kN			Ultimate Deflection, mm			Initial Stiffness [2], N/mm			Failure Mode [3]	
Model ID	Test	Model	Model -Test Ratio	Test	Model	Model-Test Ratio	Test	Model	Model-Test Ratio	Test	Model
1FL-C96	21.8	20.3	0.93	20.9	22.0	1.05	1210	985	0.81	B-WFT	B-WFT
2FL-C96	38.8	39.6	1.02	28.5	29.7	1.04	1781	1453	0.82	B-WFT	CS
3FL-C96	43.5	40.7	0.94	28.6	23.5	0.82	1975	1791	0.91	CS	CS
Average			0.96			0.97			0.85		

[1] *Ultimate load for core shear failure is based on upper bound core shear failure,* $\tau_{cu,u}$

[2] *Initial stiffnesses were calculated between deflections of 3 mm and 6 mm*

[3] *B-WFT = tensile rupture of bottom face in weft direction; CS = core shear failure*

Table 2. Parametric study results for two-way sandwich panels

Model ID	Core Density kg/m^3	Core Thickness mm	Flax Layers	Load Diameter mm	Ultimate Load kN	Ultimate Deflection mm	Stiffness N/mm	Failure Mode
1FL-C32	32	76.2	1	150	7.7	23.7	309	CW
2FL-C32	32	76.2	2	150	15.1	31.8	366	CW
3FL-C32	32	76.2	3	150	26.9	40.4	408	CW
1FL-C64	64	76.2	1	150	14.3	21.6	724	CW
2FL-C64	64	76.2	2	150	24.7	26.1	970	CW
3FL-C64	64	76.2	3	150	37.5	30.9	1133	CW
1FL-C96	96	76.2	1	150	20.3	22.0	985	TR
2FL-C96	96	76.2	2	150	39.6	29.7	1453	CS
3FL-C96	96	76.2	3	150	40.7	23.5	1791	CS
1FL-C96-L300	96	76.2	1	300	37.9	28.7	1420	TR
2FL-C96-L300	96	76.2	2	300	54.1	27.8	2090	CS
3FL-C96-L300	96	76.2	3	300	56.8	22.8	2515	CS
1FL-C96-L600	96	76.2	1	600	76.4	37.7	2266	TR
2FL-C96-L600	96	76.2	2	600	101.1	29.4	3692	CS
3FL-C96-L600	96	76.2	3	600	108.4	22.5	4677	CS
1FL-C96-CT25	96	25.4	1	150	9.3	46.7	172	TR
2FL-C96-CT25	96	25.4	2	150	11.8	34.6	302	CS
3FL-C96-CT25	96	25.4	3	150	12.2	26.2	424	CS
1FL-C96-CT51	96	50.8	1	150	14.9	29.2	516	TR
2FL-C96-CT51	96	50.8	2	150	19.1	23.9	807	CS
3FL-C96-CT51	96	50.8	3	150	20.6	19.8	1040	CS

Naming convention: XFL-CYY-(LZZZ or CT##): X is number of FFRP layers, YY is core density, ZZZ is load area diameter (optional), ## is nominal core thickness (optional)
CW = Compression Wrinkling, TR = Tensile Rupture, CS = Core Shear

LIST OF FIGURES

Figure 16. Visual comparison of (a) core Tresca stress in FE model and (b) experimental failure [Note: white color in (a) represents core Tresca stress > ultimate core shear strength (upper bound)]

Figure 17. Verification of FE models

Figure 18. Beam FE model

Figure 19. Load-deflection verification of sandwich beam FE models

Figure 20. Parametric study results (a) effect of core density; (b) effect of FFRP face thickness; (c) effect of load area diameter; and (d) effect of core thickness

Figure 21. Effect of core density on load-deflection and load-strain behaviour of two-way sandwich panels (Note: TR = Tensile Rupture, CS = Core Shear and CW = Compression Wrinkling)

Figure 22. Comparison of models with different load size diameters

Figure 23. Effect of load size diameter on load-deflection and load-strain behaviour of two-way sandwich panels (Note: TR = Tensile Rupture, CS = Core Shear and CW = Compression Wrinkling)

Figure 24. Comparison of models with different core thicknesses

Figure 25. Effect of core thickness on load-displacement and load-strain behaviour of two-way sandwich panels

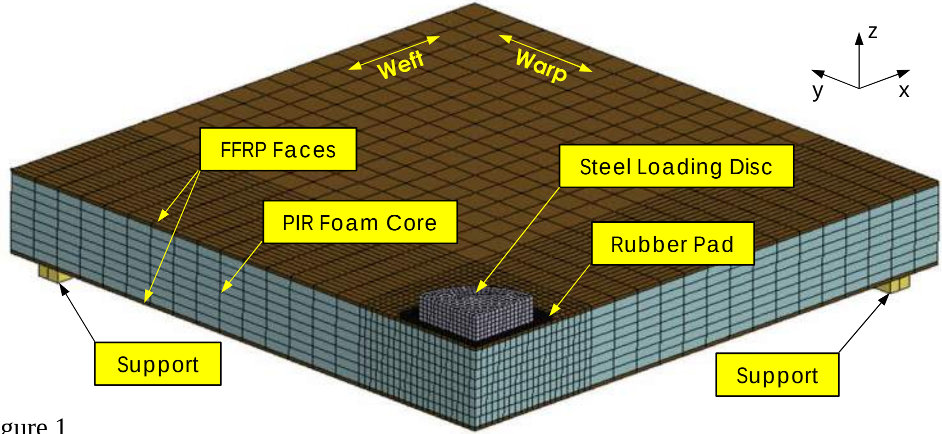
Weft
Warp
z
y
x
FFRP Faces
Steel Loading Disc
PIR Foam Core
Rubber Pad
Support
Support

Figure 1

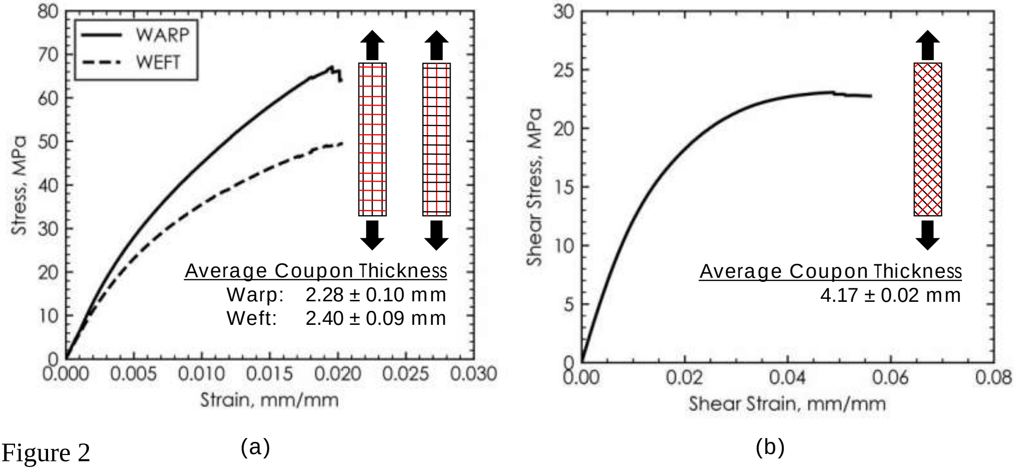
WARP
WEFT
Stress, MPa
Strain, mm/mm
Average Coupon Thickness
Warp: 2.28 ± 0.10 mm
Weft: 2.40 ± 0.09 mm
Shear Stress, MPa
Shear Strain, mm/mm
Average Coupon Thickness
4.17 ± 0.02 mm
(a)
(b)

Figure 2

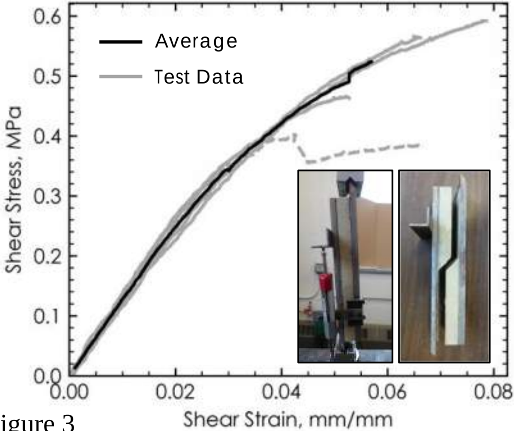
Average
Test Data
Shear Stress, MPa
Shear Strain, mm/mm
0.0
0.1
0.2
0.3
0.4
0.5
0.6
0.00
0.02
0.04
0.06
0.08

Figure 3

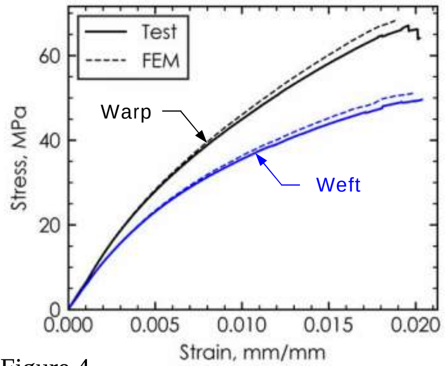
Test
FEM
60
40
20
0
Warp
Weft
Stress, MPa
0.000
0.005
0.010
0.015
0.020
Strain, mm/mm

Figure 4

Figure 5

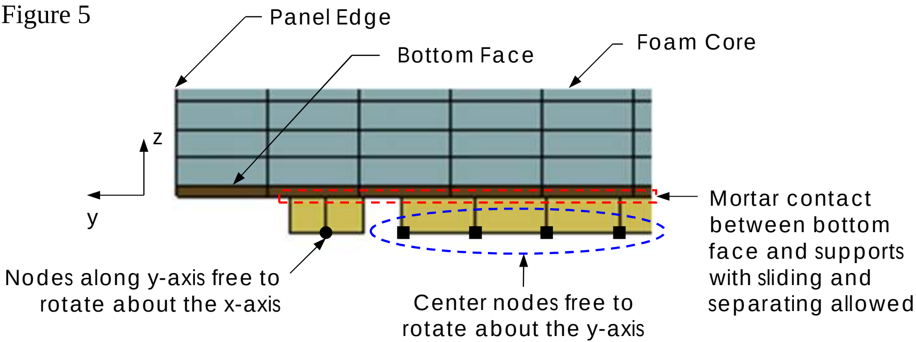
Panel Edge
Bottom Face
Foam Core
z
y
Mortar contact between bottom face and supports with sliding and separating allowed
Nodes along y-axis free to rotate about the x-axis
Center nodes free to rotate about the y-axis

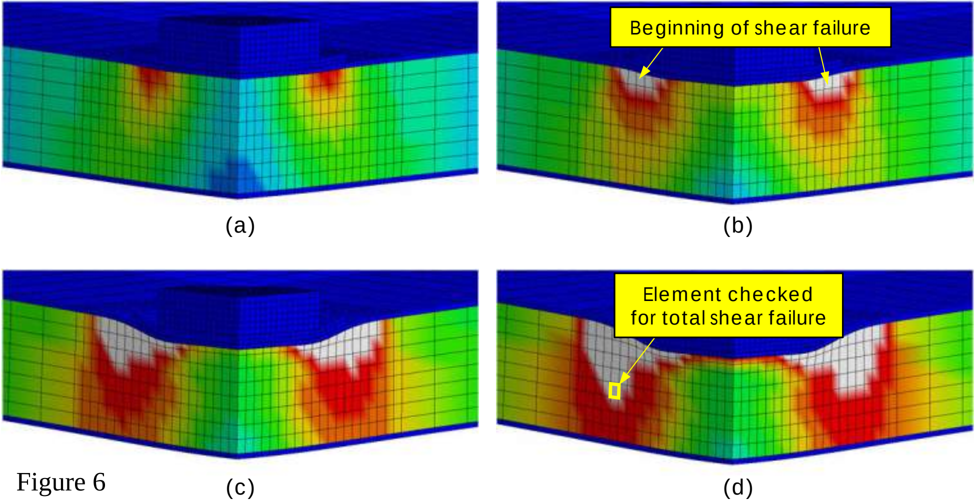
Beginning of shear failure
Element checked
for total shear failure
(a)
(b)
(c)
(d)

Figure 6

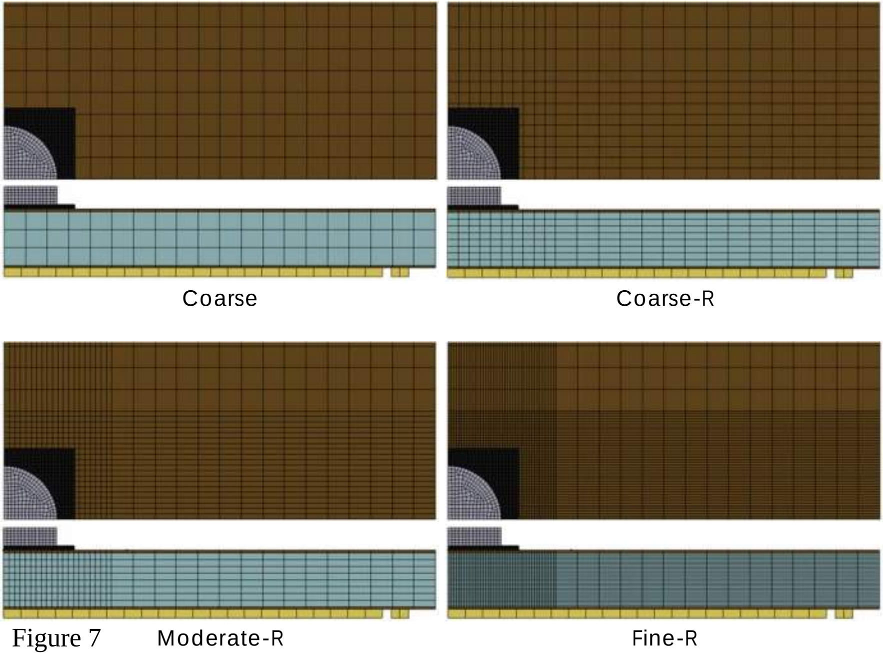

Figure 7

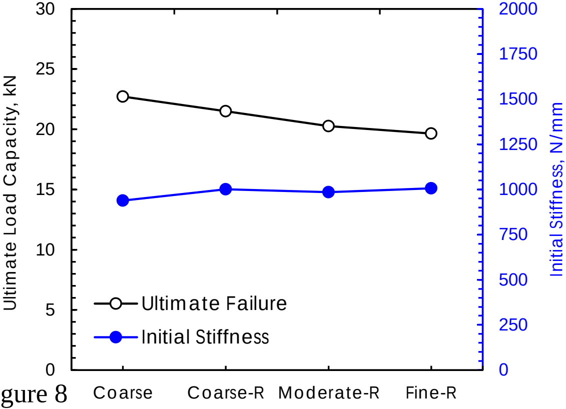

30
25
20
15
10
5
0
Ultimate Load Capacity, kN
2000
1750
1500
1250
1000
750
500
250
0
Initial Stiffness, N/mm
Ultimate Failure
Initial Stiffness
Coarse
Coarse-R
Moderate-R
Fine-R

Figure 8

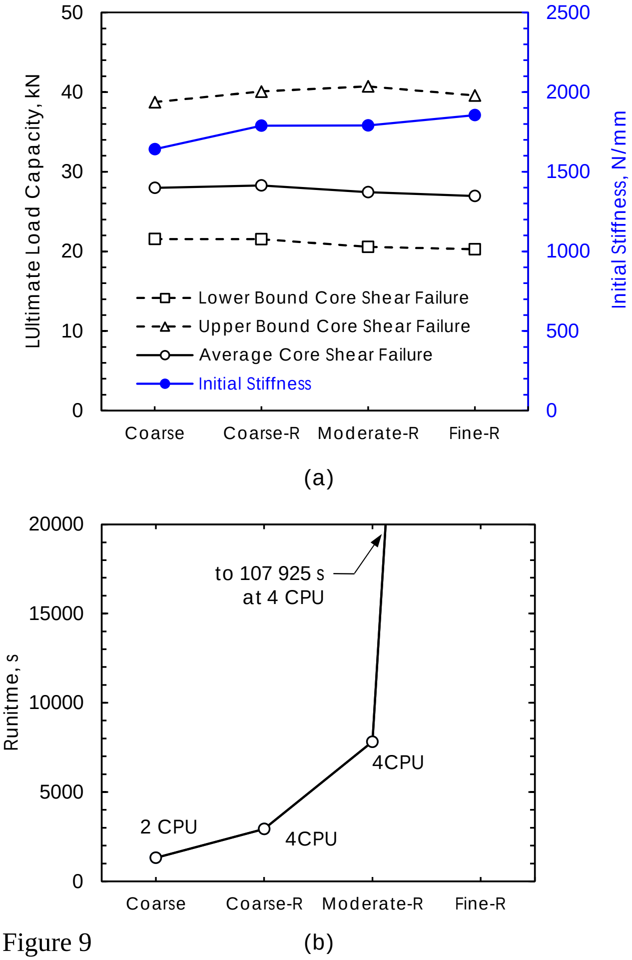

50
40
30
20
10
0
2500
2000
1500
1000
500
0
LUltimate Load Capacity, kN
Initial Stiffness, N/mm
Lower Bound Core Shear Failure
Upper Bound Core Shear Failure
Average Core Shear Failure
Initial Stiffness
Coarse
Coarse-R
Moderate-R
Fine-R
(a)
20000
15000
10000
5000
0
Runitme, s
to 107 925 s
at 4 CPU
2 CPU
4CPU
4CPU
Coarse
Coarse-R
Moderate-R
Fine-R
(b)

Figure 9

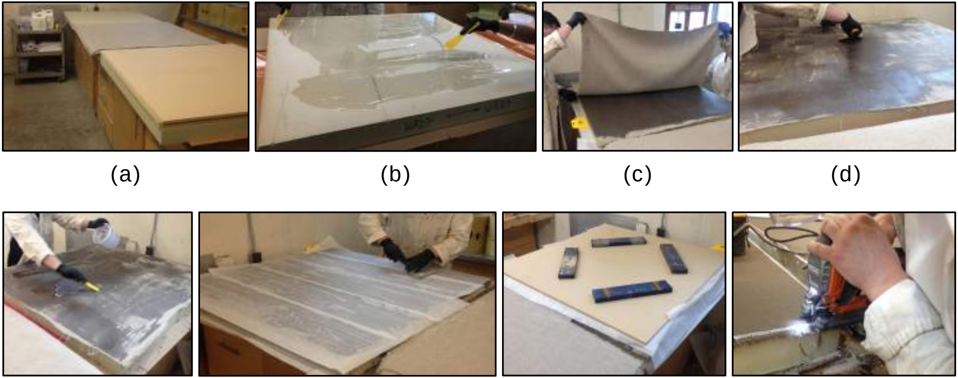

Figure 10 (e) (f) (g) (h)

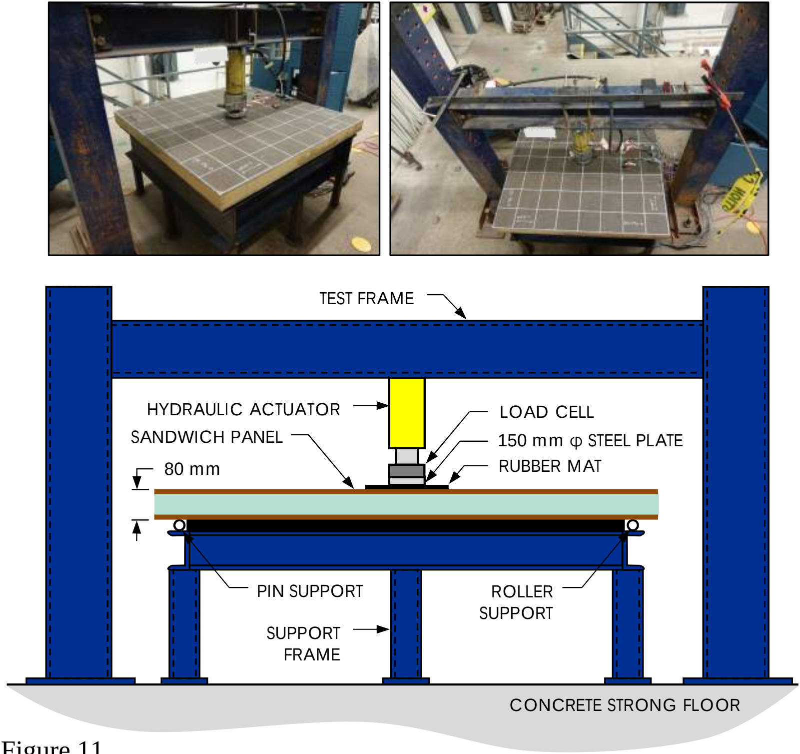
TEST FRAME
HYDRAULIC ACTUATOR
LOAD CELL
SANDWICH PANEL
150 mm φ STEEL PLATE
80 mm
RUBBER MAT
PIN SUPPORT
ROLLER SUPPORT
SUPPORT FRAME
CONCRETE STRONG FLOOR

Figure 11

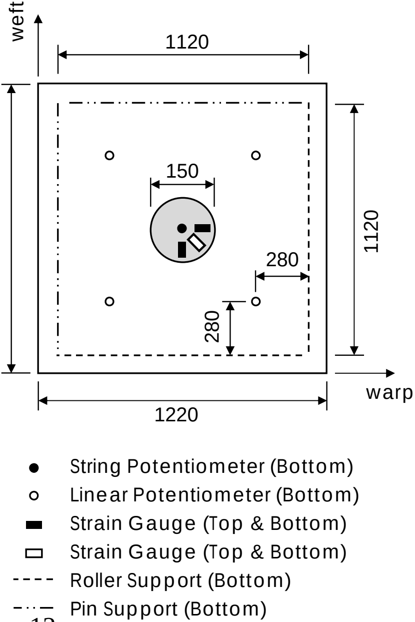

weft
1120
1220
150
1120
280
280
warp
1220
String Potentiometer (Bottom)
Linear Potentiometer (Bottom)
Strain Gauge (Top & Bottom)
Strain Gauge (Top & Bottom)
Roller Support (Bottom)
Pin Support (Bottom)

Figure 12

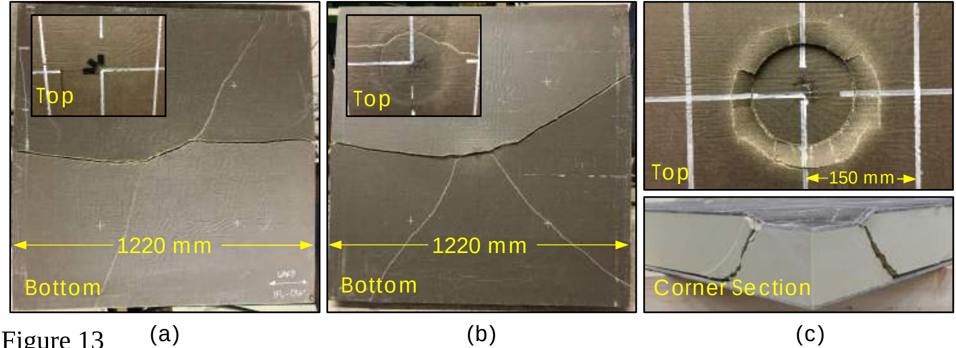

Top
1220 mm
Bottom
Top
1220 mm
Bottom
Top
150 mm
Corner Section
(a)
(b)
(c)

Figure 13

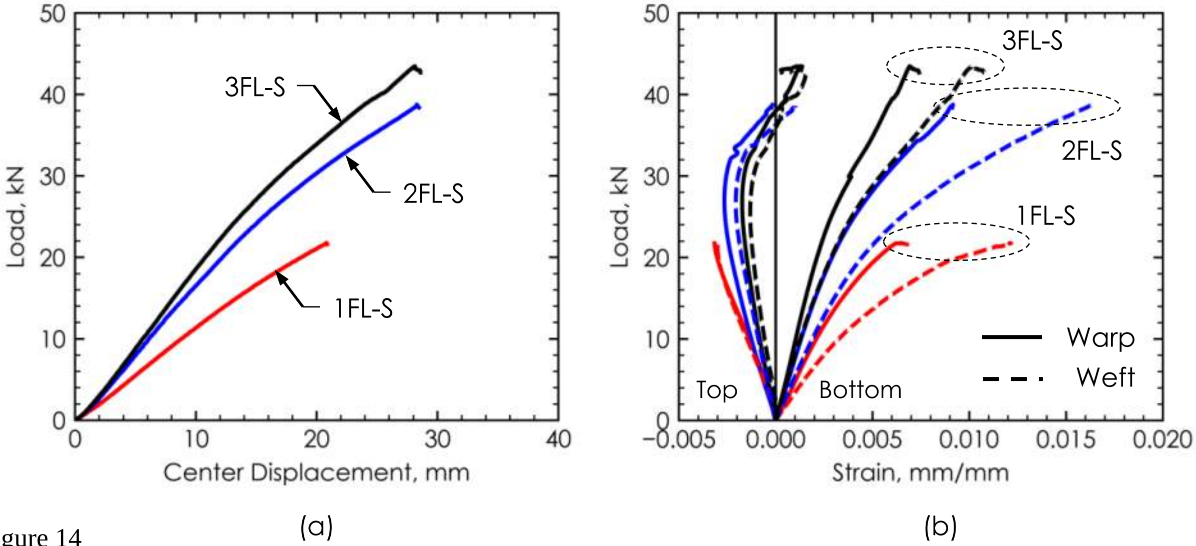
3FL-S
2FL-S
1FL-S
Load, kN
Center Displacement, mm
0
10
20
30
40
50
(a)
3FL-S
2FL-S
1FL-S
Warp
Weft
Top
Bottom
Load, kN
Strain, mm/mm
−0.005
0.000
0.005
0.010
0.015
0.020
(b)

Figure 14

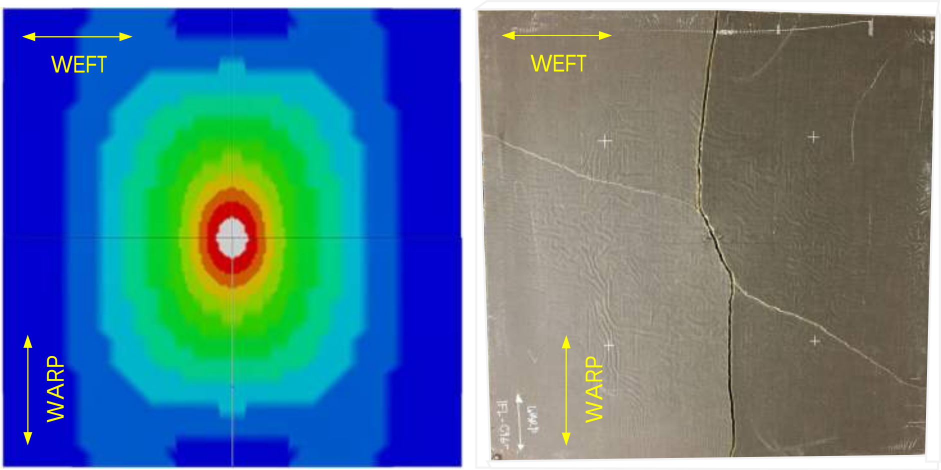

Figure 15 (a) (b)

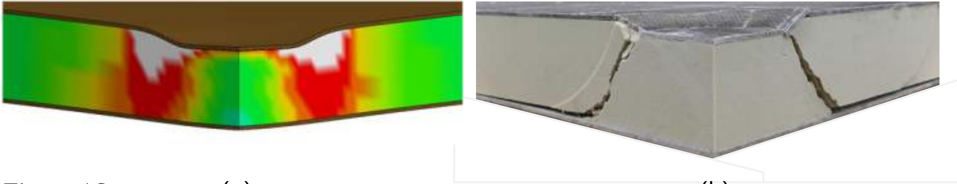

Figure 16 (a) (b)

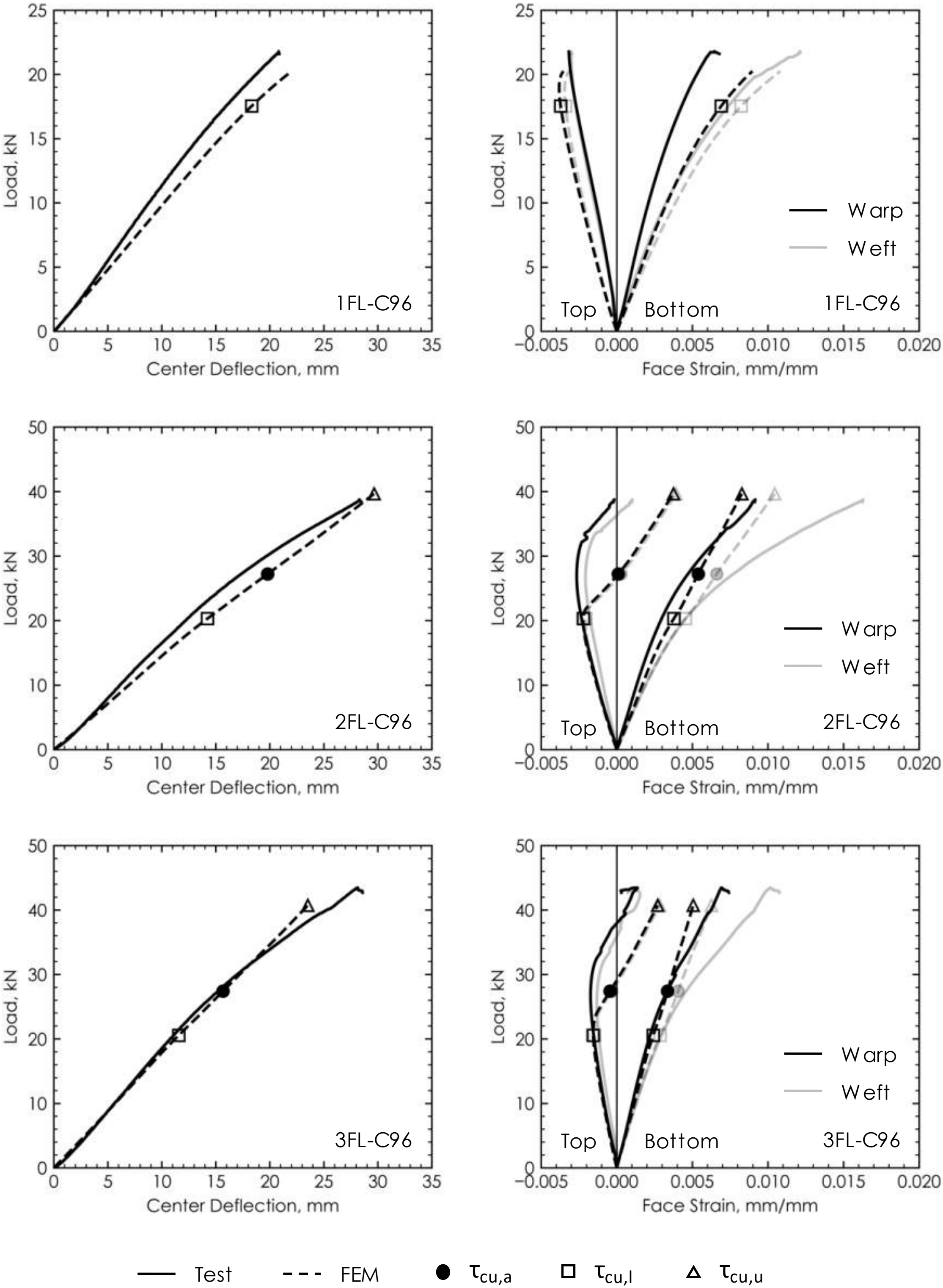

Load, kN
Center Deflection, mm
1FL-C96
Face Strain, mm/mm
Warp
Weft
Top
Bottom
1FL-C96
2FL-C96
2FL-C96
3FL-C96
3FL-C96
Test
FEM
$\tau_{cu,a}$
$\tau_{cu,l}$
$\tau_{cu,u}$

Figure 17

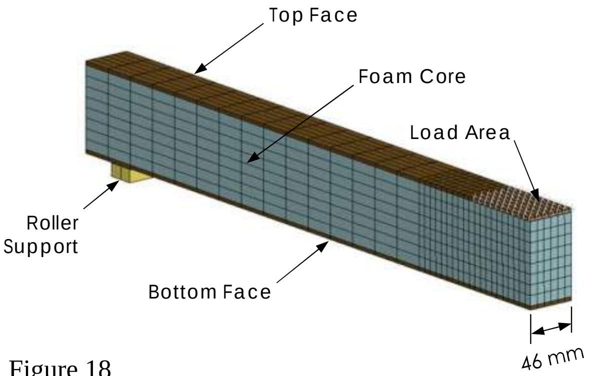

Top Face
Foam Core
Load Area
Roller
Support
Bottom Face
46 mm

Figure 18

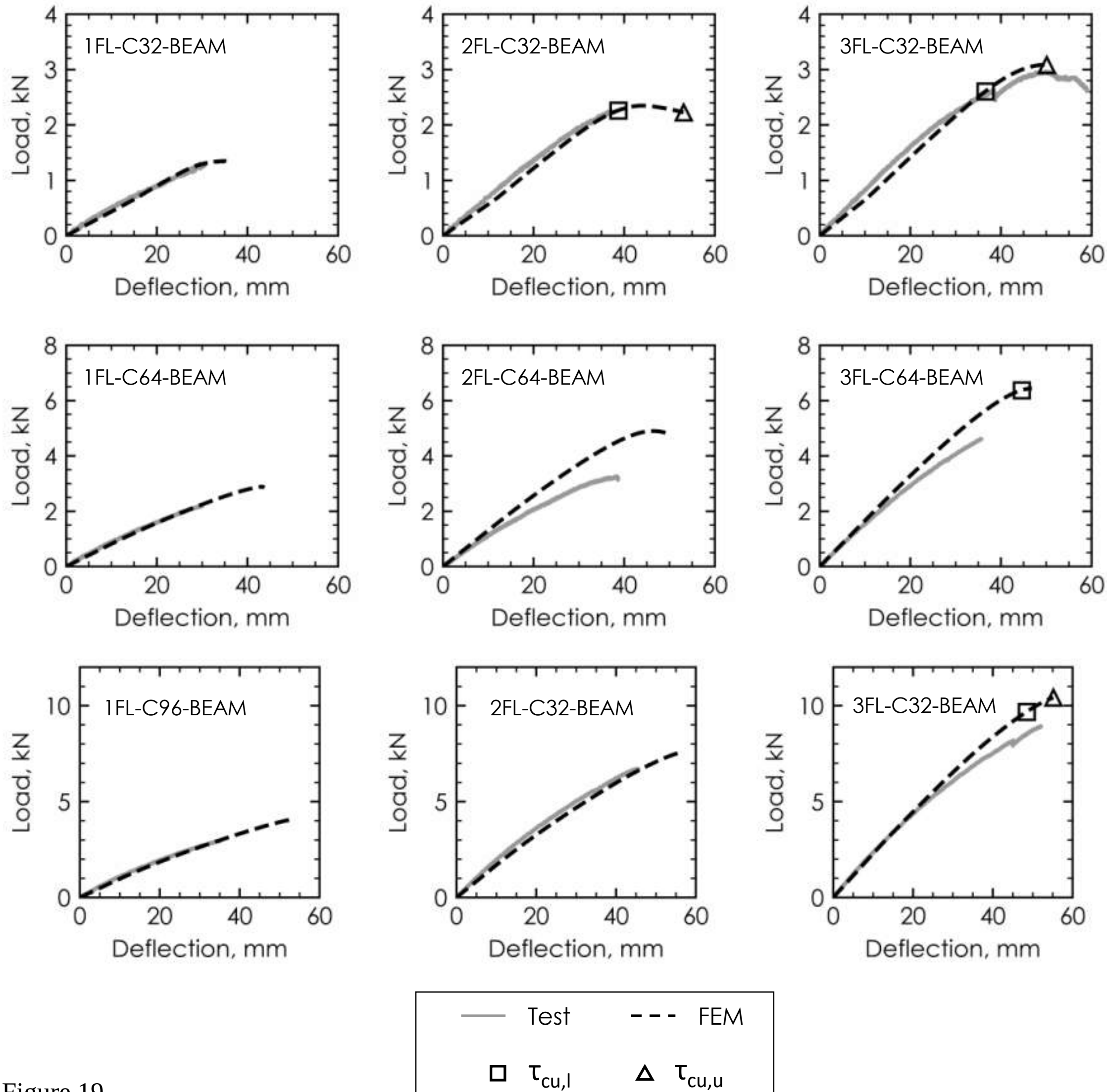
1FL-C32-BEAM
2FL-C32-BEAM
3FL-C32-BEAM
1FL-C64-BEAM
2FL-C64-BEAM
3FL-C64-BEAM
1FL-C96-BEAM
2FL-C32-BEAM
3FL-C32-BEAM
Load, kN
Deflection, mm
Test
FEM
$\tau_{cu,l}$
$\tau_{cu,u}$

Figure 19

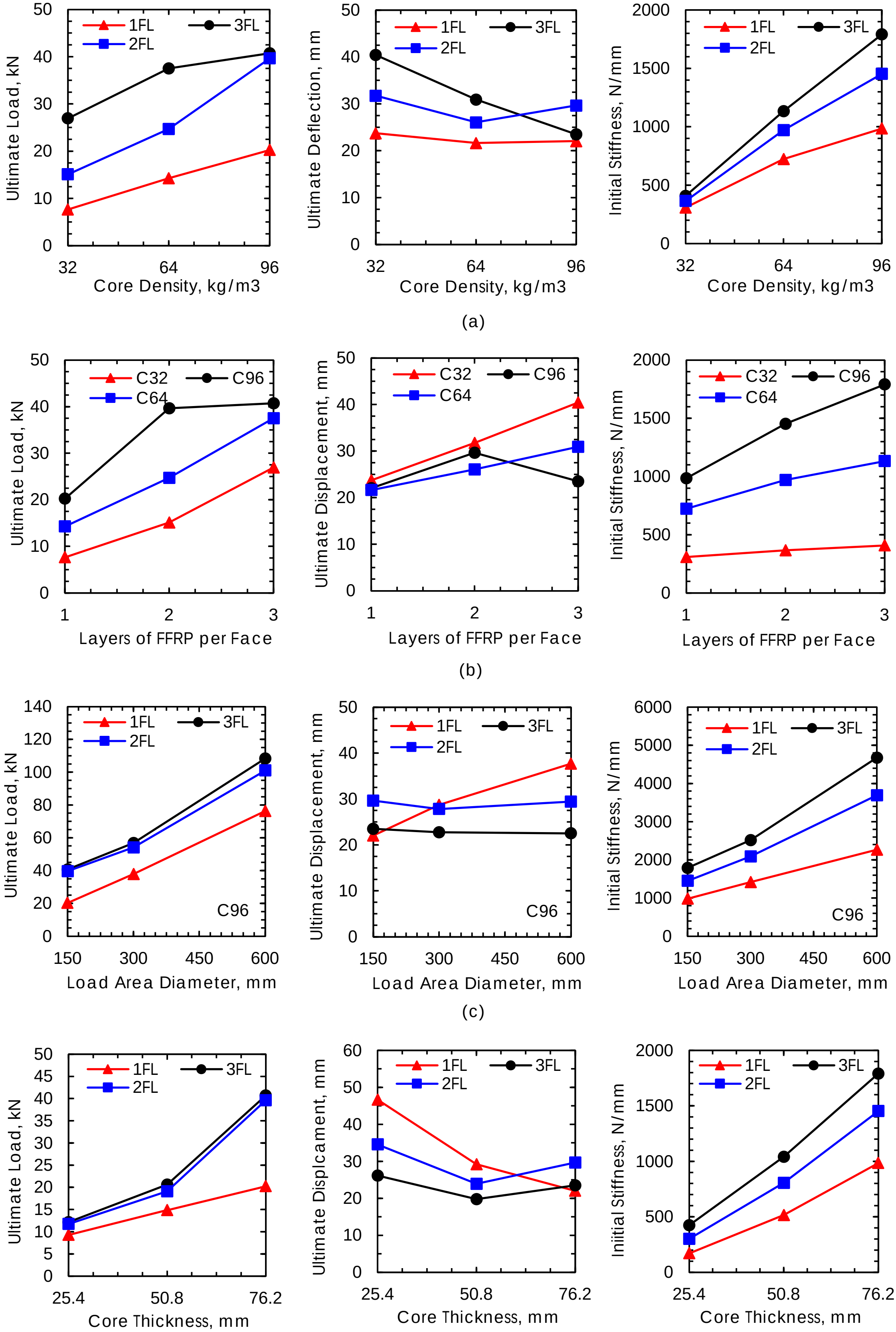

Ultimate Load, kN
Ultimate Deflection, mm
Initial Stiffness, N/mm
Core Density, kg/m3
1FL
2FL
3FL
(a)
Ultimate Load, kN
Ultimate Displacement, mm
Initial Stiffness, N/mm
Layers of FFRP per Face
C32
C64
C96
(b)
Ultimate Load, kN
Ultimate Displacement, mm
Initial Stiffness, N/mm
Load Area Diameter, mm
1FL
2FL
3FL
C96
(c)
Ultimate Load, kN
Ultimate Displcament, mm
Initial Stiffness, N/mm
Core Thickness, mm
1FL
2FL
3FL
(d)

Figure 20

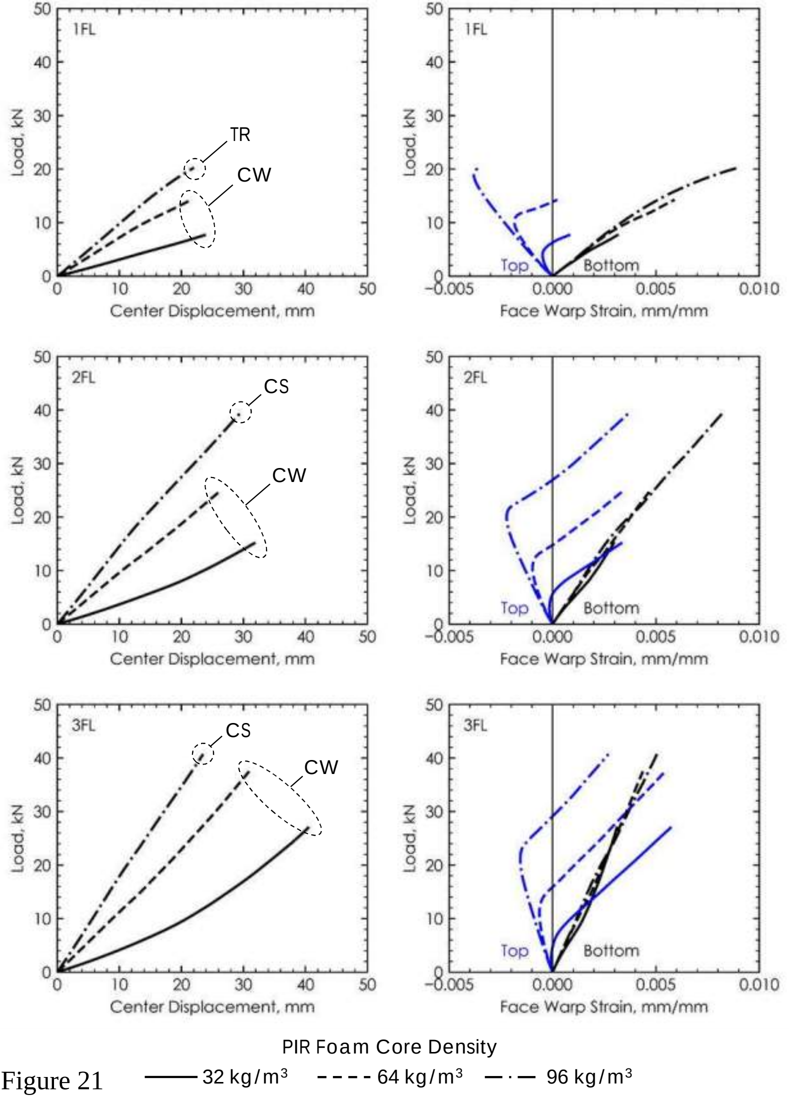

1FL
TR
CW
Load, kN
Center Displacement, mm
1FL
Top
Bottom
Load, kN
Face Warp Strain, mm/mm
2FL
CS
CW
Load, kN
Center Displacement, mm
2FL
Top
Bottom
Load, kN
Face Warp Strain, mm/mm
3FL
CS
CW
Load, kN
Center Displacement, mm
3FL
Top
Bottom
Load, kN
Face Warp Strain, mm/mm
PIR Foam Core Density
32 kg/m³
64 kg/m³
96 kg/m³

Figure 21

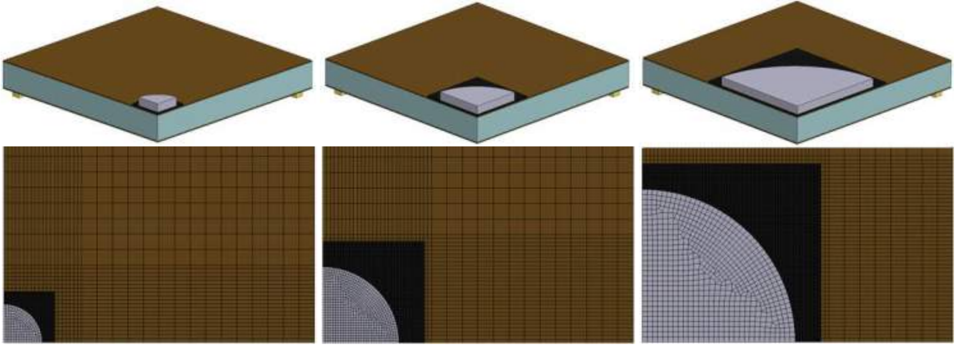

Figure 22

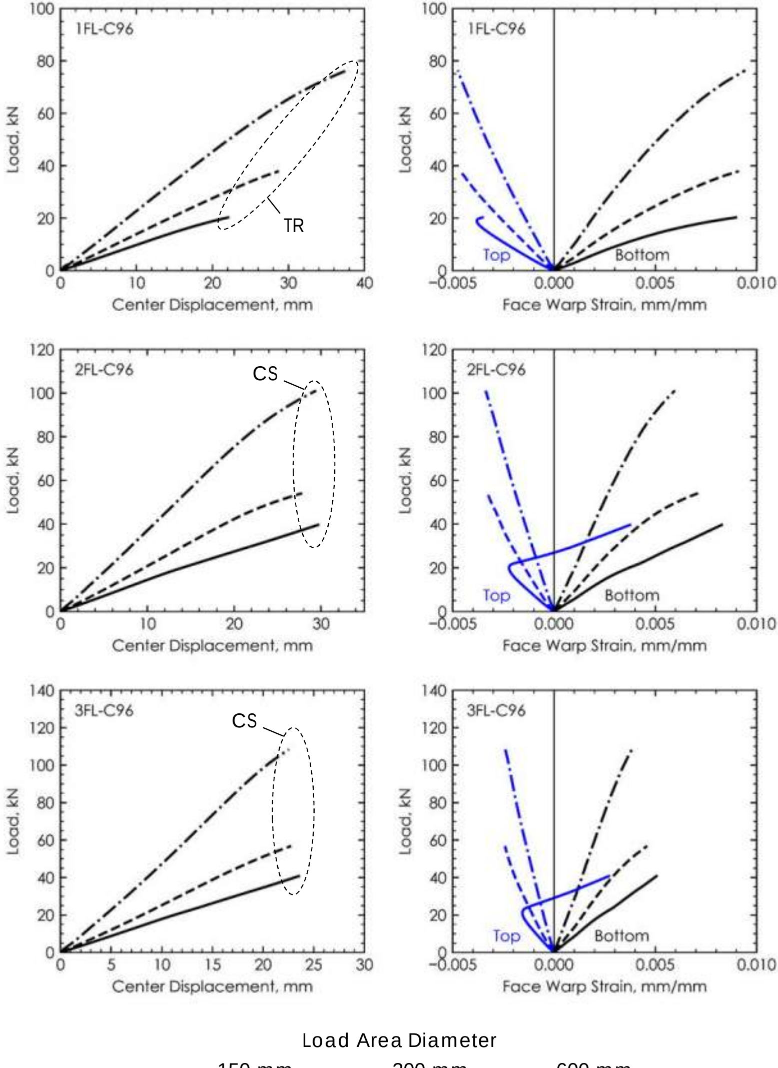
1FL-C96
TR
Load, kN
Center Displacement, mm
1FL-C96
Top
Bottom
Face Warp Strain, mm/mm
2FL-C96
CS
2FL-C96
Top
Bottom
3FL-C96
CS
3FL-C96
Top
Bottom
Load Area Diameter
150 mm
300 mm
600 mm

Figure 23

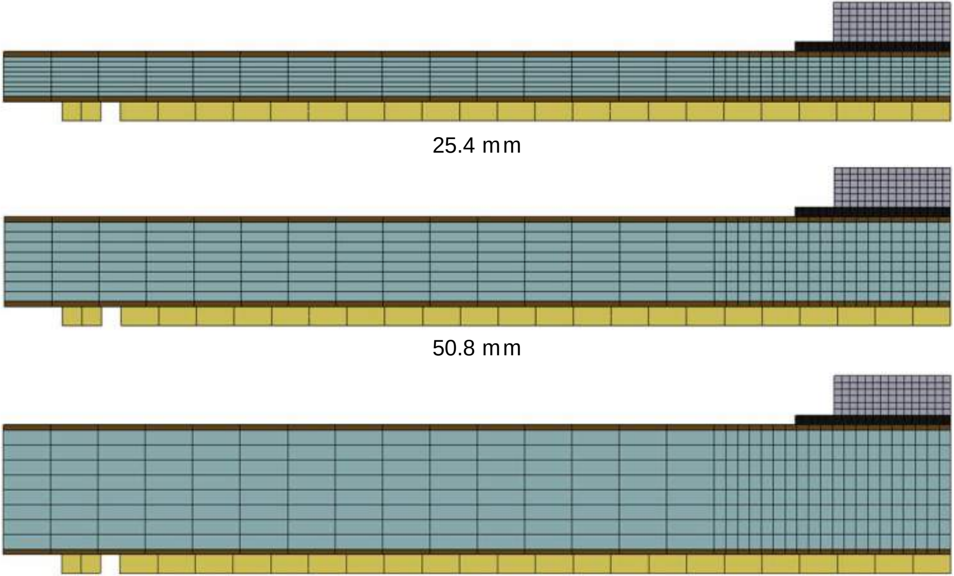

76.2 mm

Figure 24

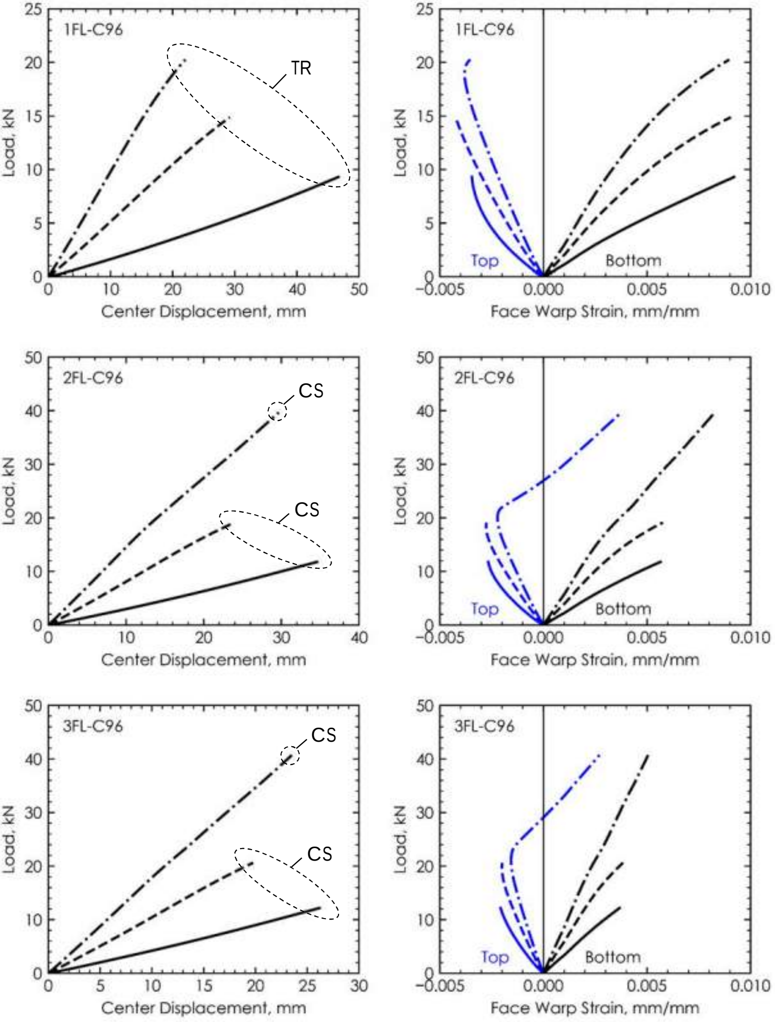

1FL-C96
TR
Load, kN
Center Displacement, mm
Face Warp Strain, mm/mm
Top
Bottom
2FL-C96
CS
CS
3FL-C96
CS
CS
Core Thickness
25.4 mm
50.8 mm
76.2 mm

Figure 25